2020 3rd IEEE International Conference on Soft Robotics (RoboSoft)
Yale University, USA

Tunable Anisotropic Stiffness with Square Fiber Jamming

Buse Aktaş[1] and Robert D. Howe[1]

***Abstract*— Jamming is a phenomenon in which a collection of compliant elements is encased in an airtight envelope, and a vacuum-induced pressure enhances frictional and kinematic coupling, resulting in dramatic changes in stiffness. This paper introduces the jamming of square cross-sectioned fibers, which allow for tunable and programmable anisotropic stiffness. A theoretical model captures the effect of major geometric design parameters on the direction-variant bending stiffness of these long and slender jamming elements. The model is experimentally validated, and a 13-fold stiffening in one direction and a 22-fold stiffening in the orthogonal direction is achieved with a single jamming element. The performance of a square-fiber-jamming continuum robot structure is demonstrated in a steering task, with an average reduction of 74% in the measured insertion force when unjammed, and a direction-variant 53% or 100% increase in the measured tip stiffness when jammed.**

Keywords: Soft Robots Material and Design, Compliance and Impedance Control, Modeling, Control, and Learning for Soft Robot

I. INTRODUCTION

Tunable stiffness allows robots to have versatile, robust, and adaptable interactions with their environments. Low stiffness allows for adaptability, conformability, and safer interactions, whereas high stiffness allows for increased forces, speed, and precision. Variable stiffness can be achieved with a variety of methods, from antagonistic actuation to shape memory alloys and spring-lever mechanisms. These structures utilize passive compliance and allow robots to undertake complex interactive tasks in unpredictable environments [1]–[5].

One mechanism that allows for tunable mechanical behavior of structures is jamming. A jamming structure consists of a collection of elements encased in an airtight bag. When a vacuum is applied to this structure, the kinematic and frictional coupling between the elements is enhanced, resulting in an increase in stiffness. Roboticists have used jamming to build devices such as conformable grippers, tunable manipulators and wearable devices [6]–[8].

Many of the studies of jamming to date have examined the jamming of layers and grains. [9], [10] There have also been a few recent studies on fiber jamming. These studies have included characterization of the jamming behavior of different material fibers, incorporation of fiber jamming structures into a surgical manipulator, and numerical analysis of the jamming transition [11]–[13]. Fiber jamming is unique, since it not only allows for better tunable bending stiffness compared to granular jamming, but also allows for more versatility compared to layer jamming by allowing tunable bending stiffness in multiple directions. This makes fiber jamming ideal for slender elements that are bending in different out-of-plane directions.

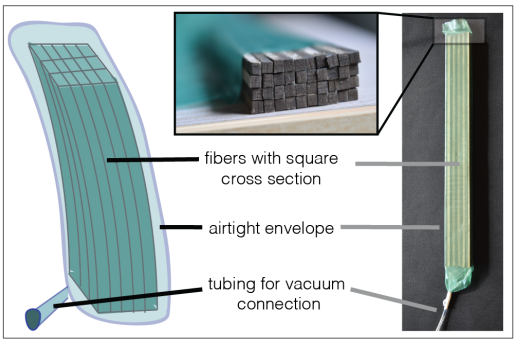

Fig. 1. Components of a square fiber jamming structure.

In this study, we specifically look at the jamming of fibers with a square cross-section, arranged in a rectangular array (Fig. 1). The square geometry of the fibers kinematically constrains them with respect to each other, allowing for a simplified theoretical model which can be utilized in designing these structures to meet particular performance criteria. Using a rectangular array of fibers as opposed to a square array allows for anisotropic mechanical behavior. The bending stiffness of the resulting structure varies in different directions, and this variation can be predetermined (programmed) by specifying geometric design parameters.

This paper begins with the characterization of the mechanical behavior of square-fiber jamming structures. The theoretical model detailing the behavior of these structures is then validated with a controlled experiment. Finally, the performance of the square jamming structure is demonstrated in a manipulation task.

II. MODELING AND CHARACTERIZATION

The theoretical model aims to relate the geometrical and material properties of a square fiber jamming structure to its bending stiffness in all directions orthogonal to the length of the fibers, capturing the effect of major design parameters. The approach taken in this new 3-D model is an extension of previous 2-D models which have been developed and validated for layer jamming structures [9].

Given a jamming structure with an n_1 by n_2 rectangular array of square fibers with thickness t, a force is applied in

This work was supported in part by the U.S. National Science Foundation National Robotics Initiative Grant CMMI-1637838.

[1] Authors are with the Paulson School of Engineering and Applied Sciences at Harvard University, Cambridge, MA, USA. buseaktas@g.harvard.edu, howe@seas.harvard.edu

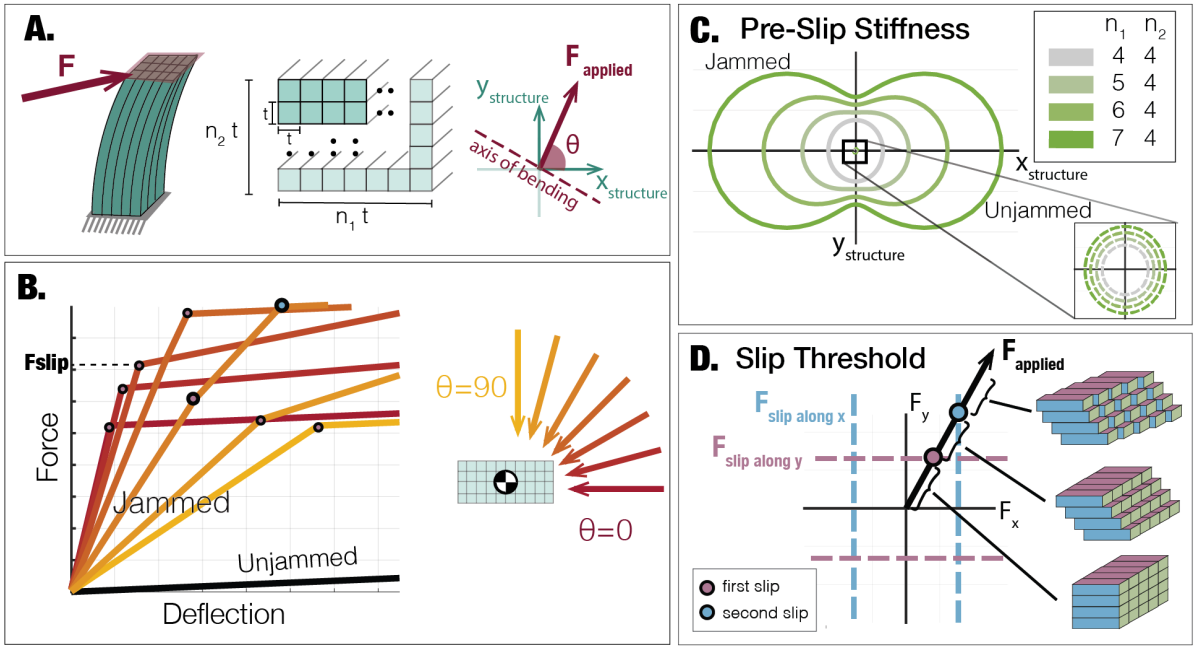

Fig. 2. Theoretical model demonstrating mechanical behavior of square fiber jamming structures. (A) The geometrical design parameters and direction of applied force. (B) Force-deflection behavior in bending along 15° increment directions. The black line shows the unjammed behavior for all seven directions. (C) Stiffness ellipses for different fiber arrangements. The unjammed stiffness is always a circle (isotropic), whereas the jammed stiffness has an anisotropy determined by the ratio of the number of fibers in the two directions. (D) The slip thresholds in two different directions. The black line shows an example case of force applied along $\theta = 60°$, in which the first slip occurs along y, and the second along x.

directions orthogonal to the length of the fibers (Fig. 2A). Bending stiffness according to Euler-Bernoulli beam theory is $k_{bending} \propto \frac{EI}{L^3}$, where E is the Young's modulus, L the distance between the supports, and I is the area moment of inertia.

In order to characterize the effect of jamming, the expressions for the area moment of inertia are derived about all possible axes, perpendicular to the direction of the force applied. It is assumed that the applied force is along the entire surface of the tip and distributed equally across all of the square fibers.

When the vacuum is not activated, the structure is unjammed and the fibers are freely sliding with respect to each other, the area moment of inertia is the sum of all the area moments of inertia of all $n_1 * n_2$ fibers. As square cross-section beams have a constant area moment of inertia in all directions, the resulting expression also does not depend on the angle (θ) along which the structure is bending:

$$I_{unjammed} = n_1 n_2 \frac{t^4}{12} \tag{1}$$

When the structure is unjammed, the bending stiffness is isotropic. Fig. 2C shows the circular stiffness ellipse in dashed lines. When a vacuum is applied, the frictional coupling between the fibers prohibits the movement of the fibers with respect to each other. Then, the structure behaves as a cohesive rectangular beam, and the area moment of inertia is that of an $n_1 t$ by $n_2 t$ cross-sectioned beam.

$$I_{jammed} = [n_1^2 cos(\theta)^2 + n_2^2 sin(\theta)^2] n_1 n_2 \frac{t^4}{12} \tag{2}$$

This results in a pre-slip stiffness dependent on θ, and the resulting anisotropic stiffness ellipse (in a shape resembling a peanut) is shown in Fig. 2C.

Equation (2) for I_{jammed} is applicable until the fibers start slipping with respect to each other, which occurs when the maximum shear stress along the beam exceeds the friction μP between the fibers. The fibers with square cross-section lead to contact surfaces in two orthogonal directions. Given an applied force F in the direction defined by θ, slip can occur along the two possible axes. We can decouple the two directions of slip and calculate the slip threshold for the two orthogonal directions:

$$F_{slip\ along\ x} = \frac{2}{3cos(\theta)} \mu P n_1 n_2 t^2 \tag{3}$$

$$F_{slip\ along\ y} = \frac{2}{3sin(\theta)} \mu P n_1 n_2 t^2 \tag{4}$$

Depending on θ, the first slip might occur in one or both directions (Fig. 2D). If the force is applied only along x, only x will slip. If the force is only applied along x, only x will slip. If the force is applied at $\theta = 45°$, then both directions will slip simultaneously. In the case of other intermediate angles, one direction will slip before the other. Fig. 2D shows a case study for $\theta = 60°$, where the fibers first slip along y, and then along x.

A simplified model for the stiffness after slip can be derived, since it is known from (3) and (4) along which axes the fibers have decoupled. At $\theta = 0°$, slip only occurs along x, at $\theta = 90°$, slip only occurs along y, and at $\theta = 45°$, slip

occurs along both along x and y simultaneously. In these three cases, the post-slip stiffness is equal to the unjammed stiffness:

$$I_{post-slip} = I_{unjammed} = n_1 n_2 \frac{t^4}{12} \tag{5}$$

Along all intermediate angles, when one slip occurs before the other, the structure has a row of fibers which are still cohesive. During this transitional phase, the structure behaves like a layer jamming structure, until the other orthogonal direction also undergoes slip (Fig. 2D). The bending stiffness during the transitional period before all fibers fully decouple can be defined by

$$I_{post\ x-slip} = \frac{n_1 n_2 t^4}{12}(cos(\theta)^2 + n_2^2 sin(\theta)^2) \tag{6}$$

$$I_{post\ y-slip} = \frac{n_1 n_2 t^4}{12}(n_1^2 cos(\theta)^2 + sin(\theta)^2) \tag{7}$$

As illustrated by the graphical representations in Fig 2, the structure behaves isotropically when unjammed, i.e. same stiffness in all directions. When jammed, there is an anisotropy based on the number of fibers along each axis, resulting in a programmable anisotropy which can be predetermined by the sample geometry.

III. Fabrication and Validation

The experimental validation of the theoretical models was performed using the setup in Fig. 3A. Square fibers were fabricated by laser-cutting $t = 2.54$ mm-thick chipboard sheets into strips with widths matching the thickness. The resulting square fibers were arranged in a 4 by 10 array, aligning the laser cut surfaces with the original surfaces at each interface in order to assure all contact surfaces had the same coefficient of friction. The array was fit into a thermoplastic elastomer sheath (Stretchlon 200, FibreGlast Developments Corp., Brookville, OH, USA), and heat-sealed to form a tight-fit pocket. An incision was made to insert tubing, and the connection was sealed with Teflon tape.

The Young's modulus of the chipboard was estimated from bending tests in two orthogonal directions. There was no significant difference between the two different directions, and the average overall modulus was 2.3 GPa. The coefficient of friction between the two surfaces was found to be $\mu = 0.6$.

In order to test the resulting jamming structure's bending stiffness in different directions, a custom three point bending fixture was fabricated (Fig. 3A). The supports for the beam were designed so that the structure could be simply supported at varying angles in 15-degree increments. The loading disk was designed to assure that the sample was loaded from its center of gravity, resulting in pure bending without inducing unwanted shear or torsion.

Force-deflection curves were obtained by mounting this fixture onto a materials testing device (Instron 5566, Illinois Tool Works, Norwood, MA, USA). The experiment was conducted at varying angles from $0°$ to $90°$ in $15°$ increments, as well as at different pressure levels: no vacuum (0 kPa) and

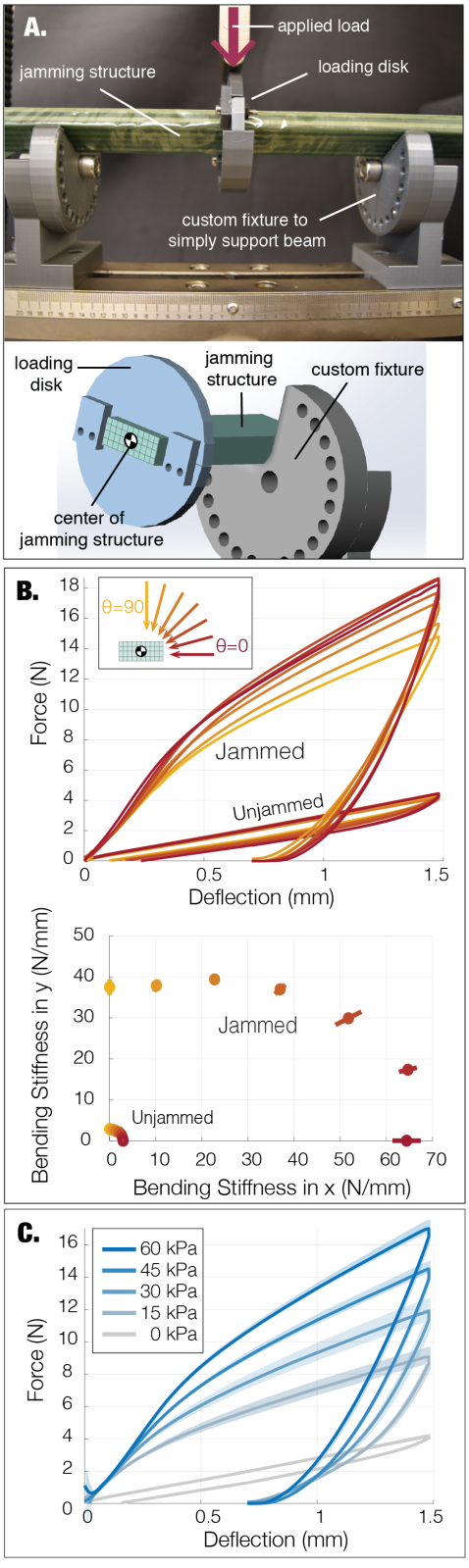

Fig. 3. Experimental behavior of square fiber jamming structures under three-point bending. (A) Experimental setup. (B) Force-deflection curve and stiffness ellipse. The error bars in the second plot show the standard deviation across trials. (C) Slip threshold is tunable with applied pressure. Shaded area shows the standard error across six trials.

vacuum (15, 30, 45, and 60 kPa). A pressure regulator (EW-07061-30, Cole-Parmer, Vernon Hills, IL, USA) controlled the vacuum level. Two different samples were tested, with three trials for each. The distance between the supports was 16.5 cm, and the maximum deflection was 1.5 mm.

The results of these experiments, shown in Figs. 3B and C, demonstrate that the unjammed bending behavior of the structure is isotropic as expected, with no significant difference between different angles and a bending stiffness of 2.9 N/mm. When the structure is jammed, the stiffness varies as the sample is rotated in the fixture, with the maximum stiffness of 64.4 N/mm at $\theta = 0°$ and the minimum stiffness of 37.5N/mm at $\theta = 90°$. This anisotropic behavior is further visualized in Fig. 2B. The peanut-shaped stiffness ellipse can be observed, corroborating the theoretical plots in Fig. 2C.

The slip behavior observed in the experiments also agreed with the aforementioned model. The points of slip were manually extracted from the average curves seen in Fig. 3B. As expected, the slip forces at $\theta = 0°$ and $\theta = 90°$ were equal to each other at 6.2 N, and the slip thresholds increased as 45° was approached from both directions.

The effect of vacuum pressure level was also measured. Fig. 3C shows the sample at a fixed angle of $\theta = 30°$ and the pressure is varied in 15 kPa increments. At 0 kPa, when the structure is unjammed, there is no slip. When jammed, for vacuum pressures 15 kPa through 60 kPa, the slip thresholds were found to be 2.3 N, 4.0 N, 6.2 N, and 9.3 N, following the scaling relationship determined by (3) and (4). This validates that the slip threshold can be tuned with the applied pressure.

The experimental results confirm the theoretical model in Section II with good repeatability. The stiffness was increased by a minimum of 13x at $\theta = 0°$ and a maximum of 23x at $\theta = 90°$, confirming not only that the structures' stiffness can be tuned over a wide range, but that it is also direction-variant.

IV. Application Example

Fiber jamming structures with variable stiffness are particularly useful for long and thin robotic manipulators. Low stiffness allows these manipulators to be easily steered through tubular structures without high contact forces (e.g. endoscopes), whereas high stiffness allows for applying high forces and providing precise position control. There have been multiple studies looking into variable-stiffness manipulators to achieve this goal, especially for surgical manipulation tasks [12], [14], [15].

To the best of our knowledge, there has been no work done on the variation of stiffness along different bending angles for manipulators. A programmable anisotropic stiffness with square-fiber jamming structures allows for versatility in tasks requiring hybrid position/force control, i.e., when precise position control is required in one direction (high stiffness) and compliant force control would be beneficial in the other direction (low stiffness).

In order to demonstrate this behavior, a continuum robot structure was fabricated from square cross-section rubber

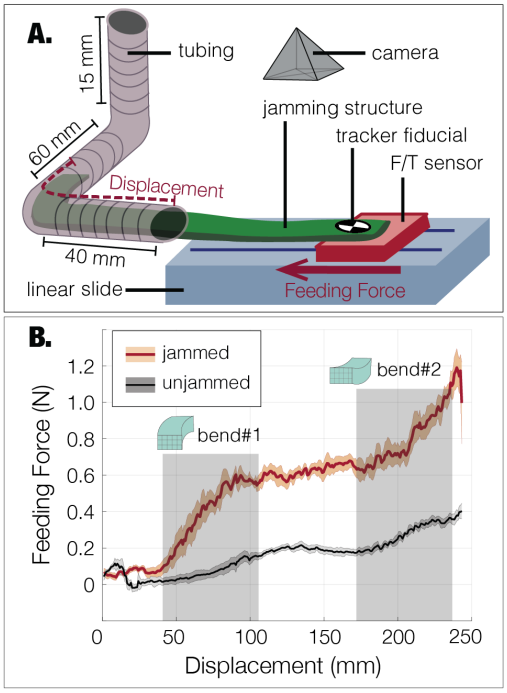

Fig. 4. Square-fiber jamming-based continuum robot structure performing a steering task, passing through bends in two orthogonal directions. (A) Experimental setup. (B) Mean insertion force as a function of displacement as the structure moves through the tube. The shaded area indicates the standard error across five trials.

fibers with a thickness $t = 2.4$ mm (SCSSIL-3/32-50, Eldon James, Denver, CO, USA). The fibers were cut into 30 cm long strips, arranged in a 3 by 5 rectangular array, fit into an elastomer sheath and attached to tubing. The continuum robot structure was first tested in a steering task to demonstrate how the variable stiffness affects the insertion force as it passes through curved paths. Once the structure made it through the path, the tip stiffness in all directions was measured both for the jammed and the unjammed states.

A. Insertion Force

Fig. 4A shows the experimental setup for measuring the insertion force as the continuum robot structure goes through a tubular path. A force sensor (HEX-58-RE-400N, OptoForce Ltd., Budapest, Hungary) was mounted on a linear slide and one side of the structure was mounted onto the sensor. Flexible plastic conduit with a smooth inner surface of inner diameter 2.1 cm (7609K4, McMaster Carr, Robbinsville, NJ, USA) was bent in two orthogonal directions, with each bend having a centerline radius of 5.2 cm. The conduit was secured with an external restraint. The external position of the structure was measured using an optical tracker (MicronTracker MTC 3.6, Claron Technology, Inc., Toronto, Canada).

The structure was manually pushed along the linear slide into the tubing. Force and position data were collected for five separate trials for both jammed and unjammed states, until the tip protruded from the other end. The force and position data were manually synchronized with each other using the onset of the motion. The five trials were then

interpolated and averaged (Fig. 4B). The insertion force was reduced by approximately a factor of three when the structure was unjammed, compared to its stiff, jammed state. This demonstrates that tuning the stiffness of the structure can control the ease of insertion through 3-D paths.

B. Tunable Tip Stiffness

Once the destination is reached without inducing high contact forces, the structure can be jammed to provide increased and anisotropic stiffness. Fig. 5A shows the experimental setup to demonstrate this behavior. An acrylic ring was placed around the outlet of the conduit, centered on the tip of the protruding manipulator, and a pulley was secured to the ring. A small light-weight cap was attached to the tip of the manipulator to provide both a secure and centered attachment for the applied force, as well as a surface to place a fiducial for tracking the position of the tip.

Force was applied to the tip by attaching a string connected to a 100 g weight of that passed through the pulley. The pulley was moved around the ring in 15-degree increments, and the manipulator's tip position was recorded using an optical tracker. There is no data on the lower right quadrant since the ring's support structure was on that side. The experiment was conducted both for the jammed manipulator and the unjammed manipulator, for three separate trials.

Fig. 5B shows all tip positions from all trials. Ellipses were fitted to the data points using the least squares method. The plot shows the deflection under a constant load and demonstrates compliance rather than stiffness, and thus we expect the inverse of what is illustrated in Fig. 2C. As expected, the unjammed state shows a much more isotropic and lower stiffness (more circular, and larger radius), whereas the jammed state results in an anisotropic and higher stiffness. The behavior was fairly repeatable, with mean standard error of 0.41 mm for the jammed state and 0.94 mm for the unjammed state at each point.

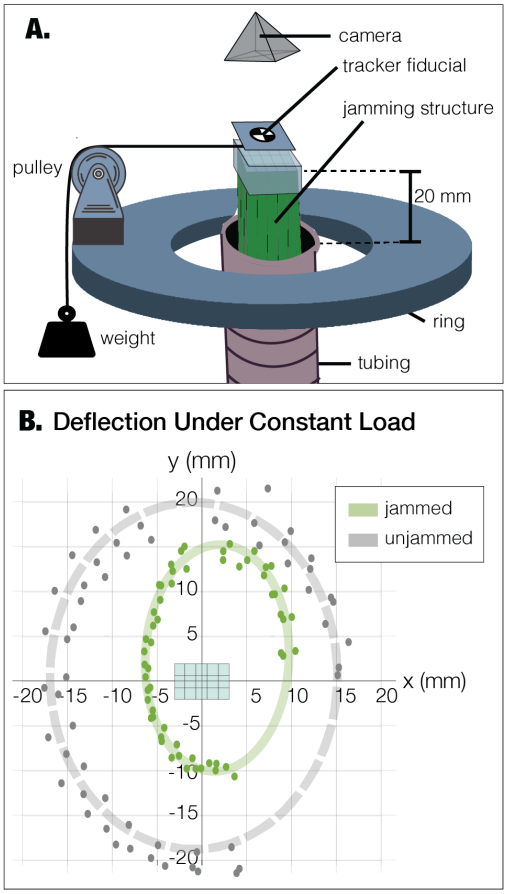

Fig. 5. Manipulator with tunable anisotropic tip stiffness. (A) Experimental setup to determine tip stiffness in all directions. (B) Experimental results showing deformation along the x-y plane.

V. Discussion and Future Work

This study introduces jamming structures with square cross-sectioned fibers, which have the advantages of other fiber jamming structures (slender variable bending stiffness elements), with the added benefit of a programmable anisotropic bending stiffness. The study also provides the first connection between a theoretical model and experimental results for fiber jamming.

The theoretical model successfully predicts the bending behavior of square fiber jamming structures given their mechanical and geometric properties. The experimentally validated behavior maps out the design space for future researchers. Finally, a tunable continuum robot structure illustrates how square jamming structures can be incorporated into long and thin robotic systems, and help provide directional force/position control while traveling through long tubular paths.

While the models capture the fundamental behavior of the fiber jamming structures, they are highly idealized. They are based on the assumption that slip along a certain axis occurs along all surfaces of that axis at once. That is why Fig. 2B has distinct linear regions, with an instantaneous change in stiffness, whereas the experimentally-observed behavior in Fig. 3B shows a more gradual transition. A more detailed model of how slip starts and perpetuates throughout the sample could be developed to incorporate the more gradual changes in stiffness during loading. In particular, with long, slender, and flexible samples such as the one used in Section IV, local slip will occur in certain regions throughout the length while other regions remain cohesive. The model could be extended to include such phenomena.

The validation experiments captured the effect of major design parameters in the model, with a particular focus on confirming the effect of bending angle θ and applied vacuum pressure P on the structure's performance. Only two different combinations for n_1 and n_2 were tested (4-by-10 for the validation experiment and 3-by-5 for the application example). Future studies could test a larger range of values to further validate the theoretical models. The validation experiment did not look at the effect of different materials (E and μ). However, previous studies have determined the effect of different constituent materials [11], [16].

The proposed model was able to predict the mechanical

behavior of these structures with reasonable accuracy, except for a few limitations. The experimental pre-slip bending stiffness about the structure's stiff axis was a factor of 4 less than the stiffness predicted by the model. This could be caused by decoupling between fibers induced by the uneven surfaces introduced during fabrication. The imperfections caused by laser-cutting can be observed in the close-up image of the cross-section in Fig. 1. Moreover, any imperfections in the orientation of the loading disk during loading (Fig. 3A) would also have an effect, as it would deviate from a pure bending scenario. These could be eliminated in future studies with higher-precision fabrication methods.

While this study only focused on tunable stiffness, as illustrated in Fig. 3C, the energy dissipation (hysteresis) of these structures can also be tuned by regulating the induced vacuum pressure. Future studies could look into the damping and frequency response of these structures as they undergo impact forces, similar to studies done in 2-D with layer jamming [17]. This exploration could be especially useful for the incorporation of these structures into robotic limbs.

The manipulator in Section IV highlights only one possible application of square fiber jamming structures. The tunable anisotropy could be utilized in other soft robotic applications. Legs with these structures would allow for a soft/unjammed state in which the robot can squeeze through small spaces, and a stiff/jammed state in which the robot can carry its weight on straight legs to achieve fast gaits and maintain lateral stability. The tunable damping behavior could be utilized to avoid high impact forces when faced with obstacles or when landing from jumps. Another possible application is fingers. Tunable anisotropy is useful for contact tasks which require compliance in the direction of contact for adaptability, and stiffness in lateral directions for precise manipulation.

In order to achieve a larger range of performance for such applications, future studies could add more versatility to the mechanical behavior of square fiber jamming by using the structures proposed here as a building block. The single-envelope structure could be used as modules, and could be stacked in two different ways: vertically along the length of the fibers, in order to independently control the stiffness of the different regions of the slender element, or orthogonal to the direction of the fibers, in order to achieve a stiffness behavior that is not simply binary. By selectively applying vacuum to different combinations of jamming elements, multiple stiffness ellipses can be achieved.

VI. Conclusions

This study introduces square fiber based jamming elements, which allow for a tunable bending stiffness with programmable anisotropy. A theoretical model is developed to capture the effect of major design parameters (geometry, material, pressure), and the model is experimentally validated. A long and slender robot continuum structure with square fiber jamming demonstrates an application. The structure allows for a tunable insertion force when steering through a curved tubular path, as well as a tunable anisotropic tip stiffness when at the target location. Square fiber jamming enables slender robotic structures with controllable anisotropic bending stiffness, which can be useful in contact tasks that require directional stiffness control.

Acknowledgments

The authors would like to thank Evelyn Park, James Weaver, Fedor Sirota and members of the Harvard Biorobotics Lab.

References

[1] S. Wolf et al., "Variable Stiffness Actuators: Review on Design and Components," *IEEE/ASME Transactions on Mechatronics*, vol. 21, no. 5, pp. 2418–2430, 2016.

[2] R. v. Ham, T. Sugar, B. Vanderborght, K. Hollander, and D. Lefeber, "Compliant actuator designs," *IEEE Robotics & Automation Magazine*, vol. 3, no. 16, pp. 81–94, 2009.

[3] M. Manti, V. Cacucciolo, and M. Cianchetti, "Stiffening in Soft Robotics," *IEEE Robotics & Automation Magazine*, pp. 93–106, 2016.

[4] L. Blanc, A. Delchambre, and P. Lambert, "Flexible Medical Devices: Review of Controllable Stiffness Solutions," *Actuators*, vol. 6, no. 3, p. 23, 2017.

[5] K. F. Laurin-Kovitz, J. E. Colgate, and S. D. Carnes, "Design of components for programmable passive impedance," in *Proceedings. 1991 IEEE International Conference on Robotics and Automation*. IEEE, 1991, pp. 1476–1481.

[6] E. Brown, N. Rodenberg, J. Amend, A. Mozeika, E. Steltz, M. R. Zakin, H. Lipson, and H. M. Jaeger, "Universal robotic gripper based on the jamming of granular material," *Proceedings of the National Academy of Sciences*, vol. 107, no. 44, pp. 18 809–18 814, 2010.

[7] J. L. C. Santiago, I. D. Walker, and I. S. Godage, "Continuum robots for space applications based on layer-jamming scales with stiffening capability," *IEEE Aerospace Conference Proceedings*, vol. 2015-June, 2015.

[8] S. Kawamura, T. Yamamoto, D. Ishida, T. Ogata, Y. Nakayama, O. Tabata, and S. Sugiyama, "Development of passive elements with variable mechanical impedance for wearable robots," in *Proceedings 2002 IEEE International Conference on Robotics and Automation (Cat. No. 02CH37292)*, vol. 1. IEEE, 2002, pp. 248–253.

[9] Y. S. Narang, J. J. Vlassak, and R. D. Howe, "Mechanically Versatile Soft Machines through Laminar Jamming," *Advanced Functional Materials*, vol. 28, no. 17, p. 1707136, 2018.

[10] H. M. Jaeger, "Celebrating soft matter's 10th anniversary: Toward jamming by design," *Soft matter*, vol. 11, no. 1, pp. 12–27, 2015.

[11] M. Brancadoro, M. Manti, S. Tognarelli, and M. Cianchetti, "Preliminary experimental study on variable stiffness structures based on fiber jamming for soft robots," *2018 IEEE International Conference on Soft Robotics, RoboSoft 2018*, pp. 258–263, 2018.

[12] M. Brancadoro, M. Manti, F. Grani, and S. Tognarelli, "Toward a Variable Stiffness Surgical Manipulator Based on Fiber Jamming Transition," vol. 6, no. March, pp. 1–12, 2019.

[13] N. Vasios, Y. Narang, B. Aktaş, R. Howe, and K. Bertoldi, "European Journal of Mechanics / A Solids Numerical analysis of periodic laminar and fibrous media undergoing a jamming transition," *European Journal of Mechanics / A Solids*, vol. 75, no. December 2018, pp. 322–329, 2019. [Online]. Available: https://doi.org/10.1016/j.euromechsol.2019.02.002

[14] M. Cianchetti, T. Ranzani, G. Gerboni, I. D. Falco, C. Laschi, S. Member, and A. Menciassi, "STIFF-FLOP Surgical Manipulator : mechanical design and experimental characterization of the single module," *2013 IEEE/RSJ International Conference on Intelligent Robots and Systems*, pp. 3576–3581, 2013.

[15] P. M. Loschak, S. F. Burke, E. Zumbro, A. R. Forelli, and R. D. Howe, "A robotic system for actively stiffening flexible manipulators," *IEEE International Conference on Intelligent Robots and Systems*, vol. 2015-Decem, no. c, pp. 216–221, 2015.

[16] Y. S. Narang, "Achieving mechanical versatility in robots and structures through laminar jamming," Ph.D. dissertation, 2018.

[17] Y. S. Narang, A. Degirmenci, J. J. Vlassak, and R. D. Howe, "Transforming the dynamic response of robotic structures and systems through laminar jamming," *IEEE Robotics and Automation Letters*, vol. 3, no. 2, pp. 688–695, 2018.